THE JOURNAL OF PHYSICAL CHEMISTRY B

ARTICLE

pubs.acs.org/JPCB

Ion Specific Effects on the Structure of Molten AF-ZrF_4 Systems ($A^+ = Li^+$, Na^+, and K^+)

Olivier Pauvert,[†,‡,§] Mathieu Salanne,*[,∥] Didier Zanghi,[†,‡] Christian Simon,[∥] Solenn Reguer,[⊥] Dominique Thiaudière,[⊥] Yoshihiro Okamoto,[#] Haruaki Matsuura,[▽] and Catherine Bessada[†,‡]

[†]CNRS-CEMHTI, 1D avenue de la Recherche Scientifique, UPR 3079, F-45071, Orléans, France

[‡]Université d'Orléans, Avenue du Parc Floral, BP 6749, F-45067, Orléans, France

[§]European Commission, Joint Research Centre, Institute for Transuranium Elements, P.O. Box 2340, D-76125, Karlsruhe, Germany

[∥]UPMC Univ Paris 06, CNRS, ESPCI, UMR 7195, PECSA, F-75005 Paris, France

[⊥]Synchrotron SOLEIL, L'Orme des Merisiers, Saint Aubin BP 48, F-91192, Gif-sur-Yvette, France

[#]Department of Materials Science, Japan Atomic Energy Research Institute, Shirakata-Shirane, Tokai-mura, Naka-gun, Ibaraki 319-1195, Japan

[▽]Research Laboratory for Nuclear Reactors, Tokyo Institute of Technology, 2-12-1 Meguro-ku, Tokyo 152-8550, Japan

ABSTRACT: The structure of AF-ZrF_4 system ($A^+ = Li^+$, Na^+, K^+) compounds in the liquid state is studied using an approach combining EXAFS spectroscopy with molecular dynamics simulations. A very good agreement is observed between the two techniques, which allows us to propose a quantitative description of the liquids. From the Zr^{4+} solvation shell point of view, we observe a progressive stabilization of the 7-fold and then of the 6-fold coordinated complexes when passing from Li^+ to Na^+ and K^+ as a "counterion". Particular attention is given to the systems consisting of 35 mol % of ZrF_4. At that particular composition, the ZrF_6^{2-} complex predominates largely whatever the nature of the alkali. The calculated vibrational properties of this complex are in excellent agreement with a previous Raman spectroscopy experiment on molten KF-ZrF_4. The most important differences are observed for the lifetime of these octahedral units, which increases importantly with the size of the monovalent cation. On a larger scale, an intense first sharp diffraction peak is observed for the $Zr^{4+}-Zr^{4+}$ partial structure factor, which can be attributed to the correlations between the octahedral units formed.

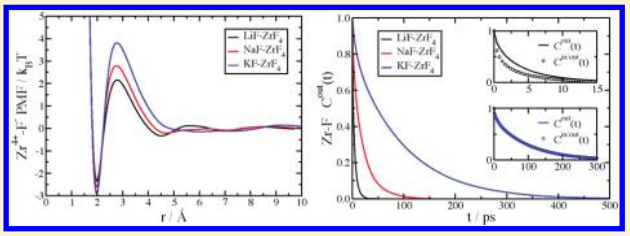

I. INTRODUCTION

Molten and glassy fluorozirconate systems play an important role in many technological applications. First, ZrF_4 is a major component of the heavy metal fluoride glasses which are used in optical fibers.[1] The interest for these materials is due to their broad optical transmission window. Second, a molten salt based on a mixture of NaF and ZrF_4 at the eutectic composition is a potential candidate to be used as primary coolant in the advanced high-temperature reactor because of its relatively low melting temperature and its good thermal properties.[2] More indirectly, important efforts have recently been devoted to the design of a molten salt fast reactor. In this generation IV nuclear reactor, the molten salt which acts both as a fuel and a coolant is made of a mixture of LiF with ThF_4.[3,4] The fuel salt is reprocessed online in order to remove the various fission products.[5−7] Zirconium compounds are investigated in this framework because of the isovalency between the Zr^{4+} and Th^{4+} ions: Studies involving the latter are more difficult to setup for issues related to its radioactivity, so that LiF-ZrF_4 is used as a "model" in preliminary studies.[8,9]

Because of these current and potential applications, the ZrF_4-based systems have attracted more attention from the scientific community than most of the other fluoride compounds. Many studies focused on the glassy compounds,[10] but the molten state has also been investigated. In particular, important informations on the structure were gathered from Raman spectroscopy experiments for the LiF-NaF-ZrF_4 and KF-ZrF_4 mixtures.[11,12] For the former, a mixture of ZrF_6^{2-}, ZrF_7^{3-}, and ZrF_8^{4-} was deduced from the experiments,[13] whereas for the latter the 6-fold and 7-fold coordinated species only were observed.[12] The thermodynamic aspects have also been studied and discussed. Using high temperature calorimetry, Hatem et al. measured the enthalpies of formation of different AF-ZrF_4 systems ($A^+ = Li^+$, Na^+, K^+, Rb^+).[14] In each case they measured negative enthalpies of mixing. A physical thermodynamic model, introduced by Grande et al. and based on the coexistence of different Zr-based complexes (ZrF_6^{2-}, ZrF_7^{3-}, and ZrF_8^{4-}) in the melt, was able to reproduce the latter data.[15]

Received: April 5, 2011
Revised: May 27, 2011
Published: June 15, 2011

In a recent work we have showed that an approach coupling EXAFS and NMR experiments with molecular dynamics simulations was able to provide a quantitative description of the LiF-ZrF_4 mixtures on a wide range of compositions.[9] The Zr^{4+} first solvation shell was shown to change importantly when passing from Zr^{4+}-dilute to concentrated systems. In particular, an "anomalous" point was observed for $x_{ZrF_4} \approx 0.33$, i.e. when there are six fluoride anions per zirconium: An important increase of the ZrF_6^{2-} species concentration was observed for that point.

Here we apply a similar approach in order to understand the specific effects on the structure due to the chemical nature of the alkali species on the structure of the AF-ZrF_4 melts. In a first step, we compare the experimental and simulated EXAFS signals in order to validate the interaction potentials used in the molecular dynamics simulations. Then we extract some information on the Zr^{4+} solvation shells, by determining the variations of their coordination numbers with the composition of the system. The longer-range structure is then probed by calculating various partial structure factors and by interpreting the low-k features which are observed. Finally, the interplay between short-range structure and intermediate-range structure is investigated through an analysis of the evolution with the alkali ion size of the zirconium solvation shell lifetime.

II. EXPERIMENTS AND SIMULATIONS

A. EXAFS Experiments. EXAFS measurements were performed in transmission geometry at the K-edge of zirconium (17998 eV), with a double crystals Si (111) monochromator, on the BL27B beamline[16] of the Photon Factory (PF) in Tsukuba (Japan), and on the DIFFABS beamline on the SOLEIL synchrotron in Gif-Sur-Yvette (France). The spectra were collected for several AF-ZrF_4 compositions, ranging from $x_{ZrF4} = 0.0$ to 0.5. For each composition, we prepared pellets from appropriate mixtures of boron nitride and metal fluorides. The proportion of each constituent was calculated taking into account the absorption coefficient relative to the pellet thickness and using the Absorbix software.[17]

Pellets of 1 cm diameter were pressed under a pressure of 5 tons cm^{-2}, to obtain a thickness of 400 μm. They were then packed inside two plates made of pyrolytic boron nitride (PBN), tightly closed with 8 screws. This system was initially developed for EXAFS measurements in molten AF-MF_3 systems ($A^+ = Li^+$, Na^+, K^+, $M^{3+} = Y^{3+}$, La^{3+} or Lu^{3+}).[18−20] The cell[21] can be heated in a furnace with a geometry adapted to the transmission mode. The heating chamber was cooled down by water and the atmosphere inside was controlled by a helium gas flow (0.2 L min^{-1}).

On the BL27B beamline, the flux of incident and transmitted photons were detected by two ionization chambers filled in N_2 and N_2−Ar (50%) mixture, respectively. The beam spot size was 5 × 1.5 mm^2. Fixed time (1 s/point) scanning was performed in the energy range from 17.7 to 18.9 keV. For the measurements on the DIFFABS beamline, we used two Si photodiodes as detectors and we reduced the beam spot size to a surface of 930 × 170 μm^2. Scanning was performed in the energy range from 17.8 to 18.8 keV.

In both cases, the collection time of one scan was of 15 min. In order to obtain a good signal-to-noise ratio on the absorption data, we collected four scans in the liquid phase and two scans in the solid phases for each compound. The EXAFS oscillations were extracted by using Athena software.[22,23] For each experiment, the samples were heated up to 50 K above the melting temperature. We heated the melt with a 10 K min^{-1} heating rate and waited 10 min before acquisition in order to homogenize the liquid. No changes were observed in the spectrum oscillations when varying the temperature in the liquid state samples.

B. Molecular Dynamics Simulations. Molecular dynamics (MD) simulations were performed for the three AF-ZrF_4 mixtures at the same compositions (x_{ZrF_4} = 0.05, 0.10, 0.15, 0.21, 0.25, 0.30, 0.35, 0.40, 0.45, and 0.50). The interaction potential used in these simulations derives from the polarizable ion model; it is best described as the sum of four different contributions: charge−charge, dispersion, overlap repulsion, and polarization[24]

$$V^{\text{total}} = V^{\text{charge}} + V^{\text{dispersion}} + V^{\text{repulsion}} + V^{\text{polarization}} \quad (1)$$

The first three components are purely pairwise additive; first the charge−charge term is

$$V^{\text{charge}} = \sum_{i<j} \frac{q^i q^j}{r^{ij}} \quad (2)$$

where q^i is the charge on ion i and formal charges are used throughout. The dispersion component includes dipole−dipole and dipole−quadrupole terms

$$V^{\text{dispersion}} = -\sum_{i<j}\left(f_6^{ij}(r^{ij})\frac{C_6^{ij}}{(r^{ij})^6} + f_8^{ij}(r^{ij})\frac{C_8^{ij}}{(r^{ij})^8}\right) \quad (3)$$

where C_6^{ij} (C_8^{ij}) is the dipole−dipole (dipole−quadrupole) dispersion coefficient and f_n are Tang−Toennies dispersion damping functions[25] describing the short-range penetration correction to the asymptotic multipole expansion of dispersion. These functions take the form

$$f_n^{ij}(r^{ij}) = 1 - c^{ij}e^{-b^{ij}r^{ij}}\sum_{k=0}^{n}\frac{(b^{ij}r^{ij})^k}{k!} \quad (4)$$

The third term of the interaction potential, the overlap repulsion component, is given by

$$V^{\text{repulsion}} = \sum_{i<j} B^{ij}e^{-a^{ij}r^{ij}} \quad (5)$$

The polarization part of the potential includes charge-dipole and dipole−dipole terms

$$V^{\text{polarization}} = \sum_{i,j}(q^i\mu_\alpha^j f_4^{ij}(r^{ij}) - \mu_\alpha^i q^j f_4^{ji}(r^{ij}))T_\alpha^{(1)} \quad (6)$$

$$-\sum_{i,j}\mu_\alpha^i\mu_\beta^j T_{\alpha\beta}^{(2)} \quad (7)$$

$$+\sum_i \frac{1}{2\alpha^i}|\boldsymbol{\mu}^i|^2 \quad (8)$$

where $T^{(1)}$ and $T^{(2)}$ are the charge-dipole and dipole−dipole interaction tensors while α^i is the polarizability of ion i. Again, Tang−Toennies functions are included to account for the short-range damping effects. The set of induced dipoles $\{\boldsymbol{\mu}^i\}_{i\in[1,N]}$ is treated as $3N$ additional degrees of freedom of the systems. The dipoles are determined at each time step by minimization of the total polarization energy and they depend on the positions of all the atoms at the corresponding time; therefore the polarization part of the potential is a many-body term.

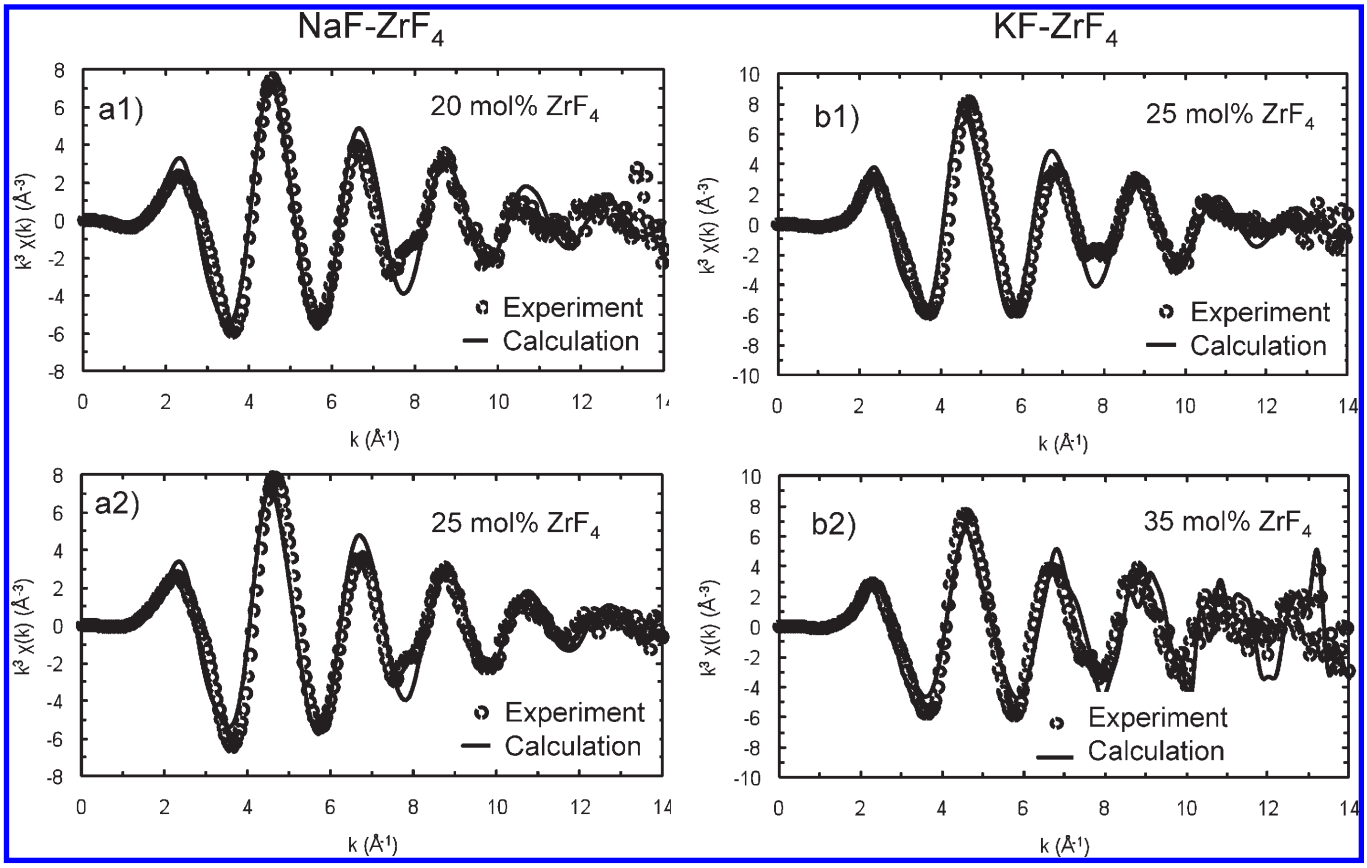

Figure 1. Comparison between the experimental and calculated EXAFS experiments. The temperatures are of 1075 K (top left), 1225 K (top right), 1125 K (bottom left), and 985 K (bottom right).

All the parameters necessary to simulate the AF-ZrF_4 mixtures have been obtained from a first-principles procedure. They are listed in ref 26. Two series of simulations have been performed. In the first one, the same temperatures were used as for the EXAFS experiments, i.e., 50 K above the melting temperature at a given composition. In the second one, the composition and temperature were respectively kept fixed at $x_{ZrF_4} = 0.35$ and $T = 1200$ K. For each temperature studied, in a first step, the equilibrium volume was determined from a simulation in the *NPT* ensemble with a target pressure of 1 atm.[27] Production runs were then performed in the *NVT* ensemble,[28] with a time step of 0.5 fs.

The total simulation time ranged between 200 ps and 2 ns. The relaxation time of the thermostat and barostat were respectively set to 10 and 5 ps. The simulation cell parameters for each composition and temperature are summarized in the Appendix. The cutoff distance for the real space part of the Ewald sum and the short-range potential was set to $L/2$ where L is the length of the side of the simulation cell. The value of the convergence parameter in the Ewald sum was set equal to $5.6/L$ and 8^3 k vectors were used for the reciprocal space part calculation of the force and potential energy.

III. RESULTS AND DISCUSSION

A. Short-Range Structure. We have first checked the ability of the MD simulations to provide a consistent picture of the structure of molten NaF-ZrF_4 and KF-ZrF_4 mixtures. It is worth noting that the interaction potentials had already been validated against thermodynamic (heat capacity, density)[26] and transport (electrical conductivity, viscosity)[26,29] properties. Concerning the structure, we have followed the same procedure as in our previous work on LiF-ZrF_4 mixtures.[9] We have calculated the EXAFS function $\chi(k)$ by using atomic configurations extracted from the MD trajectories as input data in the simulation code FEFF8.[30] The Debye−Waller factor and the anharmonic vibration effect are substituted by accumulating the MD steps in this method.[31,32] The resulting function $k^3\chi(k)$ are directly compared to the experimental ones for two NaF-ZrF_4 and KF-ZrF_4 compositions on Figure 1. The agreement between them is very satisfactory and comparable to the case of LiF-ZrF_4.[9]

The advantage of our combined approach is that the analysis of the MD trajectory provides a quantitative description of the liquids in terms of interionic distances and coordination numbers. The latter is defined by a simple geometric criterium; a fluoride anion is considered to belong to a zirconium cation first solvation shell when their interionic distance is smaller than a value $r_{cut} = 2.8$ Å which corresponds to the first minimum of the corresponding radial distribution function. In the case of LiF-ZrF_4, we observed the coexistence of three different Zr-based complexes, $[ZrF_6]^{2-}$, $[ZrF_7]^{3-}$, and $[ZrF_8]^{4-}$, which could eventually be linked together via a bridging fluoride. The concentrations of these complexes were shown to evolve smoothly, except for a composition of around 33 mol % (i.e., for which the N_{F-}/N_{Zr4+} ratio is approximately 6), for which an anomalous point was observed, with the predominance of the $[ZrF_6]^{2-}$ complex. These results are summarized in Figure 2, where they are compared to the case of NaF-ZrF_4 and KF-ZrF_4 mixtures. All

dx.doi.org/10.1021/jp203137h |*J. Phys. Chem. B* 2011, 115, 9160–9167

of the simulations were performed at a temperature of 50 K above the melting point according to the EXAFS experiments (see Table 2 in the Appendix for details); very small differences in the coordination number distributions were observed upon changing the temperature at a given composition.

When increasing the size of the alkali species, smaller coordination numbers appear to be favored: In the NaF and KF-based system, $[ZrF_8]^{4-}$ complexes are formed at high ZrF_4 concentration only ($x_{ZrF4} > 0.40$ and 0.45 respectively). The general shape of the $[ZrF_6]^{2-}$ and $[ZrF_7]^{3-}$ distributions is similar in the NaF-ZrF_4 and LiF-ZrF_4 systems, with a predominance of $[ZrF_7]^{3-}$ at low ZrF_4 amounts and of $[ZrF_6]^{2-}$ in the $x_{ZrF4} \approx 0.33$ region, but the "anomaly" is much less marked in the NaF-ZrF_4 case. The speciation is much more monotonous in KF-ZrF_4 mixtures: The main complex present is $[ZrF_6]^{2-}$ for all the studied compositions; the amount of $[ZrF_7]^{3-}$ observed remains low until $x_{ZrF4} \approx 0.45$. An illustration of the predominance of distorted octahedral complexes in KF-ZrF_4 mixtures is provided in Figure 3, where two different instantaneous configurations extracted from our MD simulations are shown.

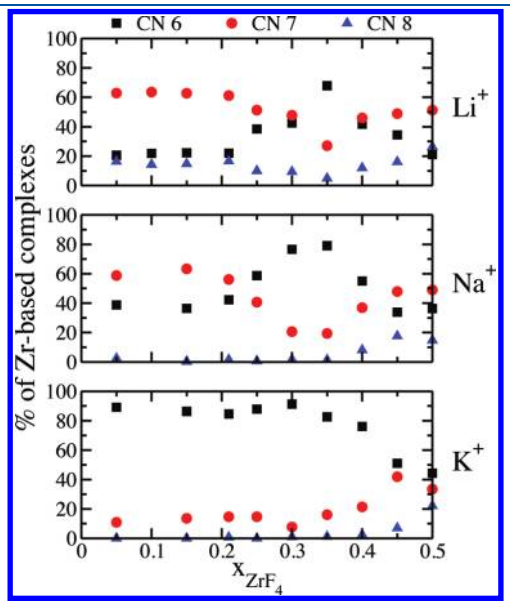

Figure 2. Evolution of the calculated coordination numbers with the composition of the melt for the three studied mixtures. CN 6, 7, and 8 respectively stand for the proportion of 6-fold, 7-fold, and 8-fold coordinated zirconium ions. All of the simulations were performed at a temperature of 50 K above the melting point according to the EXAFS experiments (see Table 2 in the Appendix for details). Reported values have a typical error bar of 1%.

In a Raman spectroscopy study on molten KF-ZrF_4 mixtures, Dracopoulos et al. have also deduced the predominance of some 6-fold coordinated Zr^{4+} ions, with smaller amounts of 7-fold coordinated ones. Our results therefore agree with this previous work. In principle, it is possible to calculate the Raman spectrum from MD simulations.[33−37] Nevertheless, such calculations would involve an important work for parametrizing a polarizability model for the F^- ions for all compositions,[38] which is beyond the scope of present work. Instead, we have chosen to follow the approach of Pavlatou et al., which consists in calculating the density of states associated with the symmetry coordinates of the octahedral ZrF_6^{2-} units and compare them with the spectroscopic observations.[39] For an octahedral "molecule", A_{1g} symmetric stretching, F_{2g} bending, E_g and F_{1u} stretching vibrational modes are expected. From our simulations, we may obtain velocities associated with the vibrational symmetry coordinates of each ZrF_6^{2-} unit. For example, for the symmetric stretching motion

$$V^i_{A_{1g}} = \sum_{i\alpha=1}^{6} v^{\parallel}_{i\alpha} \qquad (9)$$

where i labels the Zr^{4+} of a complex, $i\alpha$ the six fluoride anions contained in the octahedra, and $v^{\parallel}_{i\alpha}$ is the projection of the

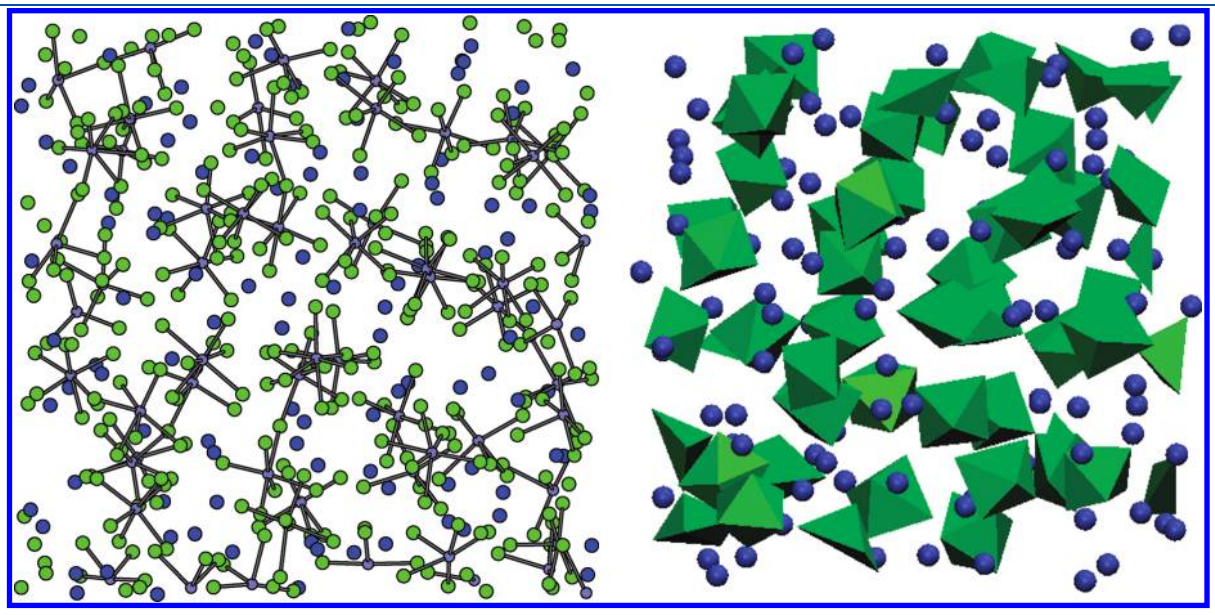

Figure 3. Molecular graphics snapshots of instantaneous configurations extracted from the simulation of the KF-ZrF_4 mixture (T = 1200 K, x_{ZrF4} = 0.35). (Left) Dark blue: K^+ ions, light blue: Zr^{4+} ions, green: F^- ions. The Zr^{4+}−F^- pairs separated by a distance lower than the first minimum of the corresponding radial distribution function (2.8 Å) are shown as bonds. (Right) Blue: K^+ ions. The Zr^{4+} coordination complexes are shown as green polyhedra.

dx.doi.org/10.1021/jp203137h |J. Phys. Chem. B 2011, 115, 9160–9167

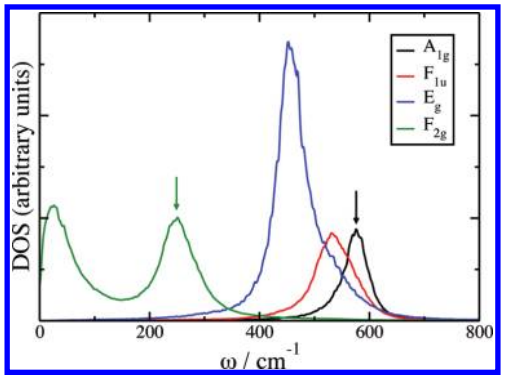

Figure 4. Octahedral normal mode vibrational DOS spectra for the KF-ZrF_4 mixture (T = 1200 K, x_{ZrF4} = 0.35). Positions of the experimentally observed Raman bands[12] (T = 1173 K, x_{ZrF4} = 0.33) are indicated by arrows.

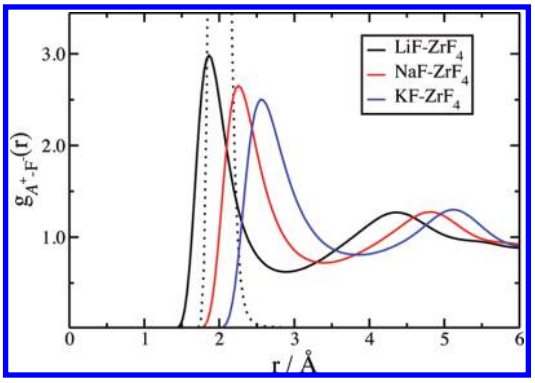

Figure 5. Full line: A^+-F^- radial distribution functions in the AF-ZrF_4 mixtures (T = 1200 K, x_{ZrF4} = 0.35). Dashed line: $Zr^{4+}-F^-$ radial distribution function first peak.

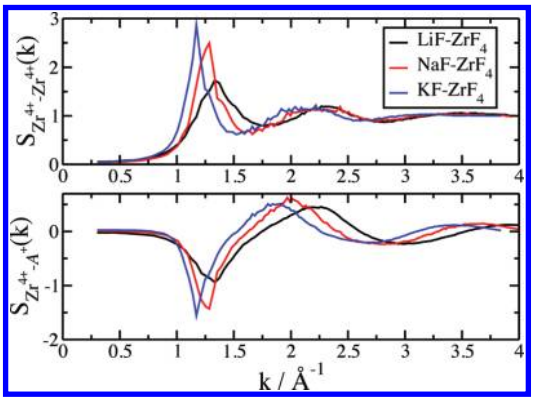

Figure 6. Partial structure factors for the AF-ZrF_4 mixtures (T = 1200 K, x_{ZrF4} = 0.35).

relative velocity of $i\alpha$ along the $Zr^{4+}-F^-$ bond. Similar expressions for the velocities of the other symmetry coordinates may be found in ref 39. The corresponding density of states is then obtained by a Fourier transform of the corresponding velocity autocorrelation function

$$\mathrm{DOS_A}(\omega) = \mathscr{R}\int_0^\infty e^{i\omega t}\langle V_A^i(t)V_A^i(0)\rangle\, dt \qquad (10)$$

The DOS obtained for the KF-ZrF_4 mixture with x_{ZrF4} = 0.35 (T = 1200 K) is shown in Figure 4. The four modes present some well-separated bands, showing that the corresponding vibrations occur at different frequencies. In the same figure, we indicate with arrows the positions of the main bands observed by Dracopoulos et al. in their Raman spectroscopy study of the x_{ZrF4} = 0.33 mixture at T = 1173 K. They correspond exactly to the maximum of our A_{1g} and F_{2g} symmetry coordinate bands, which confirms the original interpretation of the authors of the experimental study (the F_{1u} symmetry mode is Raman-forbidden and the E_g one probably has a low contribution in the overall intensity of the Raman spectrum). It also shows that not only do our simulations depict well the coordination state of the Zr^{4+} ions but also that the vibrational properties are very well predicted.

B. Intermediate-Range Structure. Although the coordination numbers change importantly when varying the nature of the alkali species, around the x_{ZrF4} = 0.33 composition the 6-fold coordinated complex is largely predominant in all cases. From a first solvation-shell point of view, one could therefore think that the three melts have similar structures at this composition. Such a result is somewhat unexpected: It is well-known that the nature of alkali cations has an important impact on the network-forming ability in ionic systems.[40] The larger the ionic radii of the alkali, the more difficult it is to incorporate in the network. Following the strong/fragile terminology introduced by Angell, the fluid then becomes more fragile.[41,42] The structure maker/breaker character of several alkali ions has also been studied in liquid water.[43] The A^+-F^- partial radial distribution functions are provided in Figure 5 for the various AF-ZrF_4 mixtures (T = 1200 K, x_{ZrF4} = 0.35). By comparing them to the $Zr^{4+}-F^-$ corresponding function first peak (shown as a dashed line), we immediatly see that the Li^+-F^- is the only pair for which the interionic distance is smaller than the $Zr^{4+}-F^-$ one. We therefore expect that the structure is less perturbed in this system than in NaF-ZrF_4 and KF-ZrF_4 compared to the structure which would be obtained in pure ZrF_4 (if this compound was stable in the liquid state).

In order to get more insight on the longer-ranged structure, we have calculated the partial structure factors for all AF-ZrF_4 mixtures, at the same composition. These were obtained from

$$S_{\alpha\beta}(k) = \frac{1}{\sqrt{N_\alpha N_\beta}}\Big\langle \sum_{i\in\alpha}\sum_{j\in\beta} e^{i\mathbf{k}\cdot\mathbf{r}_{ij}}\Big\rangle \qquad (11)$$

where $\mathbf{k}$ is a reciprocal lattice vector of the simulated system. The presence of a peak for a given wavevector k in the structure factor is due to correlations arising at a distance $R \equiv 2\pi/k$ in the real space, so that these functions usually provide more information on the intermediate and long-range correlations in a fluid than the radial distribution functions. In simple liquids, like hard-spheres or simple AX molten salts the structure factors are dominated by a principal peak, but as soon as more complex systems are studied, "prepeaks" or first sharp diffraction peaks start to be observed.[44,45] The $Zr^{4+}-Zr^{4+}$ and $Zr^{4+}-A^+$ partial structure factors are shown in Figure 6. The former is characterized by first, a broad peak at $k \approx 2.0-2.4$ Å^{-1}, which correspond to the nearest neighbors correlations and can be associated to the formation of corner-shared $Zr_2F_x^{8-x}$ units in the melt[9]

dx.doi.org/10.1021/jp203137h |J. Phys. Chem. B 2011, 115, 9160–9167

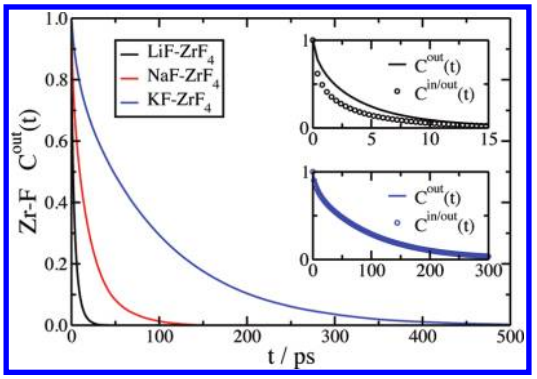

Figure 7. Cage-out correlation functions for the Zr^{4+} ions solvation shell in the AF-ZrF_4 mixtures (T = 1200 K, x_{ZrF4} = 0.35). Inset: comparison of the cage-out and cage-in-or-out correlation functions in the LiF-ZrF_4 (top) and KF-ZrF_4 (bottom) cases.

and second an intense first sharp diffraction peak at k = 1.34, 1.29, and 1.17 $Å^{-1}$ for A^+ = Li^+, Na^+, and K^+ respectively. The intensity increases along with the size of the alkali cation. It is accompanied by a minimum of the corresponding $Zr^{4+}-A^+$ partial structure factor.

Such a situation can be paralleled to the case of mixtures made with LiCl or RbCl and the network former $ZnCl_2$.[40,46] Madden and Wilson showed that the RbCl-$ZnCl_2$ system with x_{ZnCl2} = 0.33 has a similar structure to the one of a generic molten salt Rb_2T where T^{2-} is a doubly charged spherical anion with a radius mimicking the one of the $ZnCl_4^{2-}$ anion by comparing the corresponding structure factors to the $T^{2-}-T^{2-}$ and Rb^+-T^{2-} ones. As soon as Rb^+ ions are replaced by Li^+ ones, this observation does not hold anymore because those are not able to disrupt the $ZnCl_2$ network.

In the present work, the presence of an intense first sharp diffraction peak for all alkali ions supports the picture of a structure of a generic A_2T-type, where T^{2-} stands for the ZrF_6^{2-} ion. The more typical example is the KF-ZrF_4, for which the first sharp diffraction peak is the most intense; such a structure appears clearly on the second snapshot provided on figure 3. The shift of the position of the peak toward lower k values indicates that the corresponding $Zr^{4+}-Zr^{4+}$ correlations occur at larger separations. The ZrF_6^{2-} units thus become more distant, due to the higher ionic radii of the alkali ions that stand between them.

C. Lifetime of the Zr^{4+} Solvation Shell. The rate of the break-up of the coordination polyhedra of a species, which measures its solvation shell lifetime, can be investigated using the cage correlation function analysis.[47] The instantaneous set of neighboring fluoride anions of any zirconium cation i is defined by a neighbor list which is stored in a vector $\mathbf{l}_i(t)$ ($i \in [1,N_{Zr4+}]$). This vector has a dimension N_{F-}; the jth component equals 1 if the corresponding anion lies within the first coordination shell of i, and 0 otherwise. As for the coordination number, a simple geometric criteria $r_{ij} < r_{cut}$ = 2.8 Å was used to attribute the anions to the first coordination shell. Within that formalism, the number of counterions in the coordination shell of i at time t is given by $|\mathbf{l}_i(t)|^2$, and the number of ions that have left its original neighbor list in the subsequent time interval δt is

$$n_i^{out}(t, t+\delta t) = |\mathbf{l}_i(t)|^2 - \mathbf{l}_i(t)\cdot\mathbf{l}_i(t+\delta t) \qquad (12)$$

Table 1. Lifetimes τ of the Zr^{4+} First Solvation Shells Extracted from the Cage-out Correlation Functions, Activation Energies E_a as Extracted from the Potential of Mean Forces, and Diffusion Coefficients in the AF-ZrF_4 Mixtures (T = 1200 K, x_{ZrF4} = 0.35)

	τ	E_a	D_{F-}	D_{Zr4+}	D_{A+}
system	(ps)	(k_BT)	(10^{-5} cm^2 s^{-1})		
LiF-ZrF_4	3.1	4.48	2.38	1.49	7.67
NaF-ZrF_4	15.7	5.39	1.34	0.96	4.08
KF-ZrF_4	76.4	6.72	1.39	1.26	5.86

The cage-out correlation function for the Zr^{4+} ions solvation shell then is given by

$$C^{out}(t) = \frac{1}{N_{Zr^{4+}}}\langle \sum_{i=1}^{N_{F^-}} \Theta(1 - n_i^{out}(0,t))\rangle \qquad (13)$$

where Θ is the Heaviside step function. So defined, the cage-out correlation function measures the rate at which a single counterion leaves the cage. Using similar definitions, it is also possible to calculate the correlation functions measuring rates for an ion to enter into the cage (cage-in), but also for an ion to enter or to leave it (cage-in-or-out). On figure 7 we show the cage-out correlation functions for the Zr^{4+} ions solvation shell in the AF-ZrF_4 mixtures (T = 1200 K, x_{ZrF4} = 0.35). It is then possible to define a characteristic lifetime of the solvation shell as the time τ needed for the function to reach a value of 1/e.[48,49] The calculated lifetimes are provided in table 1; they increase rapidly with the size of the alkali ion.

It is possible to give a simple interpretation for the evolution of the lifetimes based on the intermediate range structure which was observed in the melts: With the increase of the alkali ion size, the ZrF_6^{2-} octahedra become more and more isolated. The decrease of the first sharp diffraction peak position in the $Zr^{4+}-Zr^{4+}$ partial structure factor is associated to a longer distance between two units. In some glassy materials for which the species migration mechanism is characterized by diffusive jumps, the longer the jump length is, the slower the ion diffuses. Although this picture does not hold here for diffusion because the systems of interest are in the liquid state, and the species are very mobile as shown by the diffusion coefficients provided in table 1, we can expect a similar mechanism to occur for the break up of the Zr^{4+} solvation cages. It is also worth noting that the fluoride/zirconium diffusion coefficient ratio decreases from 1.6 to 1.1 when passing from the Li^+ ion based mixture to the K^+ ion based one. In the second case, the solvation shell relaxation occurs on a characteristic time (76.4 ps) which is similar to the time needed for the fluoride ions to reach the diffusive régime (estimated from the time for which their mean-squared displacements become linear), while in the first case it occurs before. Therefore in the KF-ZrF_4 mixture the fluoride ions can be considered to diffuse similarly as the ZrF_6^{2-} units.

From the thermodynamic point of view, the potentials of mean force which will determine the F^- exchanges between ZrF_6^{2-} units can be evaluated by

$$PMF(r) = -k_B T\, ln\, g_{Zr^{4+}-F^-}(r) \qquad (14)$$

where k_B is Boltzmann's constant and T is the temperature of the simulation. The functions are plotted in Figure 8; they are

dx.doi.org/10.1021/jp203137h |J. Phys. Chem. B 2011, 115, 9160–9167

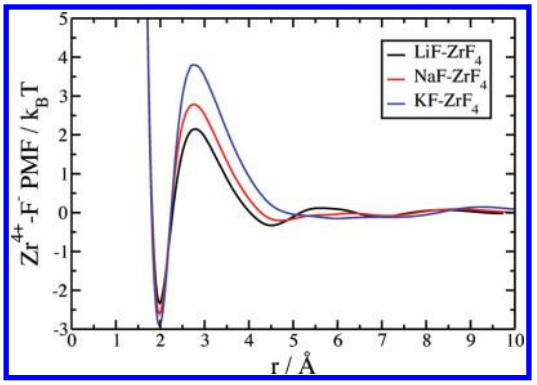

Figure 8. Potentials of mean force for the $Zr^{4+}-F^{-}$ dissociation obtained following eq 14 in the AF-ZrF_4 mixtures (T = 1200 K, x_{ZrF4} = 0.35).

characterized by a deep first minimum in all cases. The barrier for the anions escape of the first solvation shell corresponds to the energy difference between this first minimum and the following maximum. These are given in Table 1. We observe that the break-up rate $k = 1/\tau$ of the solvation shell increases with respect to this activation energy.

The comparison of the cage-out and cage-in-or-out correlation functions, which are provided for LiF-ZrF_4 and KF-ZrF_4 in the inset of Figure 7, also shows another interesting feature. In the K^+ case, we observe a similar decay rate for the two functions, which means that the F^- exchange is a concerted mechanism: As soon as one anion enters the solvation shell of a Zr^{4+} cation, another one is leaving it. On the contrary, in the Li^+ case, the decay rate differ; this is consistent with the fact that the structure is more network-like in this case.

IV. CONCLUSION

In conclusion, we have showed in this paper that the nature of the alkali cation induces important changes in the structure of AF-ZrF_4 mixtures. The Zr^{4+} solvation shell is particularly affected, with a stabilization of the ZrF_6^{2-} units relatively to the ZrF_7^{3-} and ZrF_8^{4-} ones when the ionic radii of the monovalent increase (i.e., when passing from Li^+ to Na^+ and then to K^+). Even at the x_{ZrF4} = 0.35 composition, for which the Zr^{4+} is mainly 6-fold coordinated in the three cases, further structural investigations show important differences. The larger the ionic radii of the alkali, the more difficult it is to incorporate in the original structure; the octahedral units therefore are less connected in the KF-based system. Although all the systems present a generic A_2T molten salt structure where T^{2-} stands for the ZrF_6^{2-} anion, this picture is enhanced in the case of the KF-ZrF_4 mixture, which reflects in the higher intensity of the first sharp diffraction peak in the $Zr^{4+}-Zr^{4+}$ structure factor.

The increase in the distance separating the octahedral units impacts the lifetime of the solvation shell: Fluoride anions have to jump across a higher activation energy barrier, which results in lower solvation shell break-up rates as given by the cage correlation functions. Also, we observe a concerted mechanism in the case of KF-ZrF_4 for this solvation shell break-up mechanism. The leaving of a fluoride anion occurs simultaneously to the entrance of another one, which is not observed in the LiF-ZrF_4 case.

APPENDIX A

Table 2. Molecular Dynamics Simulations Conditions[a]

x_{ZrF4}	N_{F-}	N_{Zr4+}	N_{Li+}	N_{Na+}	N_{K+}	L (Å)	T (K)
5	260	11	216	0	0	18.2	1120
10	247	19	171	0	0	17.6	1100
15	222	23	130	0	0	16.8	1070
21	273	35	133	0	0	17.6	970
25	287	41	123	0	0	18.1	1050
30	367	58	135	0	0	19.5	970
35	340	58	108	0	0	19.2	920
40	297	54	81	0	0	18.0	870
45	272	52	64	0	0	17.4	840
50	290	58	58	0	0	17.5	800
5	253	11	0	209	0	20.2	1300
15	222	23	0	130	0	18.5	1200
20	240	30	0	120	0	18.5	1075
25	245	35	0	105	0	18.8	1125
30	253	40	0	93	0	18.7	1125
35	340	58	0	108	0	20.6	1100
40	319	58	0	87	0	19.2	820
45	272	52	0	64	0	18.0	765
50	275	55	0	55	0	17.9	875
5	253	11	0	0	209	22.6	1125
15	213	22	0	0	125	20.4	1125
20	240	30	0	0	120	20.9	1225
25	231	33	0	0	99	20.5	1225
30	253	40	0	0	93	20.9	1225
35	246	42	0	0	78	19.8	985
40	253	46	0	0	69	19.3	875
45	256	49	0	0	60	19.1	775
50	260	52	0	0	52	18.7	775
35	340	58	108	0	0	19.5	1200
35	340	58	0	108	0	20.7	1200
35	340	58	0	0	108	22.7	1200

[a] The temperatures are the same as for the EXAFS experiments, except for the three simulations performed at T = 1200 K. L is the length of the side of the simulation cell.

ACKNOWLEDGMENT

The authors acknowledge the support of the French Agence Nationale de la Recherche (ANR), under Grant ANR-09-BLAN-0188 ("MILIFOX"), as well as the PCR ANSF program and the Regional Council of the Region Centre. We also thank Mr Masahiko Numakura (Tokyo Institute of Technology, Japan) for his help in our experiments on the BL27 beamlines. We would like to thank Emmanuel Véron and Sandra Ory (CEMHTI, Orléans) for XRD and DSC measurements and Dr. Anne-Laure Rollet for her contribution in the development of all the instrumentation. The EXAFS data were obtained by the experiments under the proposal numbers 2006G318 and 2008G065 (PF/KEK, Japan), 20060237, and 20080276 (SOLEIL, France). HM expresses special gratitude to the STUDIUM for enabling the collaboration study between CEMHTI, CNRS, and RLNR, Tokyo Tech.

REFERENCES

(1) Quimby, R. S., Aggarwal, I. D., Lu, G., Eds.; *Fluoride Glass and Fiber Optics*; Academic Press Inc.: Boston, 1991.

(2) Forsberg, C. *Prog. Nucl. Energy* **2005**, *47* (1−4), 32–43.
(3) Delpech, S.; Merle-Lucotte, E.; Heuer, D.; Allibert, M.; Ghetta, V.; Le-Brun, C.; Doligez, X.; Picard, G. *J. Fluorine Chem.* **2009**, *130* (1), 11–17.
(4) Benes, O.; Bellmann, M.; Konings, R. J. M. *J. Nucl. Mater.* **2010**, *405* (2), 186–198.
(5) Hamel, C.; Chamelot, P.; Laplace, A.; Walle, E.; Dugne, O.; Taxil, P. *Electrochim. Acta* **2007**, *52* (12), 3995–4003.
(6) Taxil, P.; Massot, L.; Nourry, C.; Gibilaro, M.; Chamelot, P.; Cassayre, L. *J. Fluorine Chem.* **2009**, *130* (1), 94–101.
(7) Chamelot, P.; Massot, L.; Cassayre, L.; Taxil, P. *Electrochim. Acta* **2010**, *55* (16), 4758–4764.
(8) Groult, H.; Barhoun, A.; Ghallali, H. E.; Borensztjan, S.; Lantelme, F. *J. Electrochem. Soc.* **2008**, *155* (2), E19–E25.
(9) Pauvert, O.; Zanghi, D.; Salanne, M.; Simon, C.; Rakhmatullin, A.; Matsuura, H.; Okamoto, Y.; Vivet, F.; Bessada, C. *J. Phys. Chem. B* **2010**, *114* (19), 6472.
(10) Aasland, S.; Einarsrud, M.-A.; Grande, T.; McMillan, P. F. *J. Phys. Chem.* **1996**, *100* (13), 5457–5463.
(11) Toth, L. M.; Quist, A. S.; Boyd, G. E. *J. Phys. Chem.* **1973**, *77* (11), 1384–1388.
(12) Dracopoulos, V.; Vagelatos, J.; Papatheodorou, G. *J. Chem. Soc., Dalton Trans.* **2001**, *7*, 1117–1122.
(13) Toth, L. M.; Bates, J. B.; Boyd, G. E. *J. Phys. Chem.* **1973**, *77* (2), 216–221.
(14) Hatem, G.; Tabaries, F.; Gaune-Escard, M. *Thermochim. Acta* **1989**, *149*, 15–26.
(15) Grande, T.; Aasland, S.; Julsrud, S. *J. Am. Ceram. Soc.* **1997**, *80* (6), 1405–1415.
(16) Konishi, H.; Yokoya, A.; Shiwaku, H.; Motohashi, H.; Makita, T.; Kashihara, Y.; Hashimoto, S.; Harami, T.; Sasaki, T. A.; Maeta, H.; Ohno, H.; Maezawa, H.; Asaoka, S.; Kanaya, N.; Ito, K.; Usami, N.; Kobayashi, K. *Nucl. Instrum Methods Phys. Res., Sect. A* **1996**, *372* (1−2), 322–332.
(17) Michalowicz, A.; Moscovici, J.; Muller-Bouvet, D.; Provost, K. *J. Phys. Conf. Ser.* **2009**, *190*, 012034.
(18) Rollet, A.-L.; Bessada, C.; Rakhmatullin, A.; Auger, Y.; Melin, P.; Gailhanou, M.; Thiaudière, D. *C. R. Chim.* **2004**, *7*, 1135–1140.
(19) Rollet, A.-L.; Rakhmatullin, A.; Bessada, C. *Int. J. Thermophys.* **2005**, *26*, 1115–1126.
(20) Bessada, C.; Rakhmatullin, A.; Rollet, A.-L.; Zanghi, D. *J. Fluorine Chem.* **2009**, *130* (1), 45–52.
(21) Rollet, A.-L.; Bessada, C.; Auger, Y.; Melin, P.; Gailhanou, M.; Thaudière, D. *Nucl. Instrum. Methods Phys. Res., Sect. B* **2004**, *226*, 447–452.
(22) Newville, M. *J. Synchrotron Radiat.* **2001**, *8*, 322–324.
(23) Ravel, B.; Newville, M. *J. Synchrotron Radiat.* **2005**, *12*, 537–541.
(24) Madden, P. A.; Wilson, M. *Chem. Soc. Rev.* **1996**, *25* (5), 339–350.
(25) Tang, K.; Toennies, J. *J. Chem. Phys.* **1984**, *80* (8), 3726–3741.
(26) Salanne, M.; Simon, C.; Turq, P.; Madden, P. A. *J. Fluorine Chem.* **2009**, *130* (1), 38–44.
(27) Martyna, G. J.; Tobias, D. J.; Klein, M. L. *J. Chem. Phys.* **1994**, *101* (5), 4177–4189.
(28) Martyna, G. J.; Klein, M. L.; Tuckerman, M. E. *J. Chem. Phys.* **1992**, *97* (4), 2635–2643.
(29) Salanne, M.; Simon, C.; Groult, H.; Lantelme, F.; Goto, T.; Barhoun, A. *J. Fluorine Chem.* **2009**, *130* (1), 61–66.
(30) Ankudinov, A. L.; Ravel, B.; Rehr, J. J.; Conradson, S. D. *Phys. Rev. B* **1998**, *58*, 007565.
(31) Okamoto, Y. *Nucl. Instrum. Methods Phys. Res., Sect. A* **2004**, *526*, 572–583.
(32) Okamoto, Y.; Suzuki, S.; Shiwaku, H.; Ikeda-Ohno, A.; Yaita, T.; Madden, P. *J. Phys. Chem. A* **2010**, *114* (13), 4664–4671.
(33) Madden, P. A.; Wilson, M.; Hutchinson, F. *J. Chem. Phys.* **2004**, *120* (14), 6609–6620.
(34) Glover, W.; Madden, P. *J. Chem. Phys.* **2004**, *121* (15), 7293–7303.
(35) Giacomazzi, L.; Umari, P.; Pasquarello, A. *Phys. Rev. Lett.* **2005**, *95* (7), 075505.
(36) Giacomazzi, L.; Umari, P.; Pasquarello, A. *Phys. Rev. B* **2006**, *74* (15), 155208.
(37) Giacomazzi, L.; Umari, P. *Phys. Rev. B* **2009**, *80* (14), 144201.
(38) Heaton, R. J.; Madden, P. A. *Mol. Phys.* **2008**, *106* (12−13), 1703–1719.
(39) Pavlatou, E. A.; Madden, P. A.; Wilson, M. *J. Chem. Phys.* **1997**, *107* (24), 10446–10457.
(40) Wilson, M.; Madden, P. A. *Phys. Rev. Lett.* **1994**, *72* (19), 3033–3036.
(41) Angell, C. A. *J. Non-Cryst. Solids* **1991**, *131−133*, 13–31.
(42) Wilson, M.; Salmon, P. S. *Phys. Rev. Lett.* **2009**, *103* (15), 157801.
(43) Mancinelli, R.; Botti, A.; Bruni, F.; Ricci, M. A.; Soper, A. K. *J. Phys. Chem. B* **2007**, *111*, 13570–13577.
(44) Salmon, P. S. *J. Phys.: Condens. Matter* **2006**, *18* (50), 11433–11444.
(45) Salanne, M.; Simon, C.; Turq, P.; Madden, P. A. *J. Phys.: Condens. Matter* **2008**, *20* (33), 332101.
(46) Zeidler, A.; Salmon, P. S.; Martin, R. A.; Usuki, T.; Mason, P. E.; Cuello, G. J.; Kohara, S.; Fischer, H. E. *Phys. Rev. B* **2010**, *82* (10), 104208.
(47) Rabani, E.; Gezelter, J. D.; Berne, B. J. *J. Chem. Phys.* **1997**, *107* (17), 6867–6876.
(48) Salanne, M.; Simon, C.; Turq, P.; Heaton, R. J.; Madden, P. A. *J. Phys. Chem. B* **2006**, *110* (23), 11461–11467.
(49) Salanne, M.; Simon, C.; Turq, P.; Madden, P. A. *J. Phys. Chem. B* **2007**, *111* (18), 4678–4684.